Performance Comparison of Transfer Switch Topologies in Switched-Doubly-Fed Machine Drives

Arijit Banerjee, Steven B. Leeb, and James L. Kirtley
Department of Electrical Engineering and Computer Science, Massachusetts Institute of Technology
Cambridge, Massachusetts, USA
arijit@mit.edu, sbleeb@mit.edu, kirtley@mit.edu

***Abstract*—Switched doubly-fed machines (DFM) creates variable speed drives with reduced power electronics requirements compared to shaft power, and with the additional benefit of controllable stator power factor. A solid-state transfer switch is a critical component of a switched-DFM drive that not only allows seamless shaft control across the full speed range but also permits effective grid interaction. This paper presents and compares two transfer switch topologies—twelve-thyristor-based and eight-thyristor-based that reconfigures the DFM connections on-the-fly with different shaft torque-speed demands. Reducing the number of thyristors allows the operation of the DFM with lesser commutation constraints. Appropriate control input is derived that maximizes the damping of the stator flux during the mode transition.**

I. Introduction

Variable speed drives (VSD) have wide range of applications in industrial processes, electric propulsion systems, and power generation plants [1]. In these VSDs, power converters that control the electromechanical energy conversion are mostly rated to handle the full shaft power. At higher shaft power, the power converter design becomes overly challenging due to limited available component ratings and allowable device switching frequency. For example, currently the voltage rating of IGBTs that are typically used for medium voltage drives ranges between 3.3 kV and 6.5 kV with an allowable switching frequency of a few hundred Hz [2]. Stacking multiple devices in series/parallel—as in multilevel converters—becomes a standard approach for processing power at levels beyond the available ratings of the individual devices [3], [4], [5].

Alternatively, for limited-speed range applications, high-power VSDs can be created using a reduced-sized power converter with a wound-rotor induction/doubly-fed machine (DFM). The configuration has been widely used in the wind power generation [6] where for the limited-speed range operation the power processed by the power converter is typically one-third of the full shaft power. For full-speed range applications, including electric propulsion drives, the flexibility of the DFM can be exploited with on-the-fly reconfiguration of the power connections to the stator - a configuration known as a switched-DFM drive [7]. A typical switched-DFM drive operates over a speed range of ± 1.5 p.u (normalized relative to the ac source synchronous speed) with a rotor converter power rating of a third of the maximum shaft power [8]. The reduction in the converter rating improves drive efficiency, lowers the fundamental drive frequency, reduces filter size, improves machine-side and source-side harmonics, and reduces converter cooling requirements [9]. Additionally, the switched DFM drive offers seamless interface, controllable power factor, and reactive power support to the ac grid [10]. Figure 1 shows a switched-DFM drive with a transfer switch that connects the stator windings of the DFM to multiple sources or shorts the stator windings together based on the operating speed while a back-to-back power converter controls the electromechanical energy conversion from the rotor.

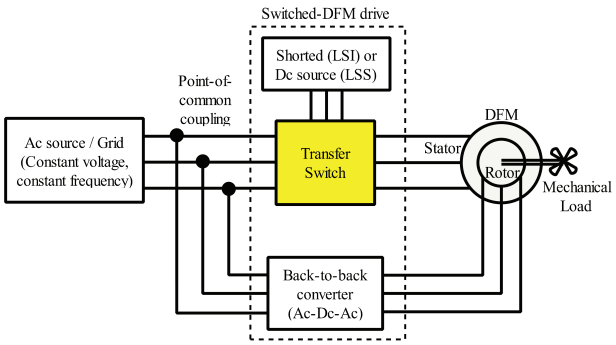

Figure 1. Typical configuration of a switched-doubly-fed machine drive.

The switched-DFM drive can operate either in the low-speed induction topology (LSI) or in the low-speed synchronous topology (LSS) [11], [12], [13] based on the possible stator winding configurations. At lower drive speed, the DFM stator is either shorted in the LSI topology or is connected to a low-voltage dc source in the LSS topology. This mode of operation of the switched-DFM drive is referred to as "low-speed" mode. At higher drive speed, in both topologies, the DFM stator is connected to the ac source/grid, which is denoted as "high-speed" mode. The mode transition speed depends on the topology as well as on the required drive torque-speed characteristic.

The transfer switch is the key enabler for a switched-DFM drive that reconfigures the stator connection on-the-fly. Although a mechanical transfer switch can potentially be used for the stator reconfiguration [11], [14], [15], this choice results in poorer reliability and transfer performance for applications that need frequent reconfigurations and seamless

978-1-4673-9550-2/16/$31.00 ©2016 IEEE

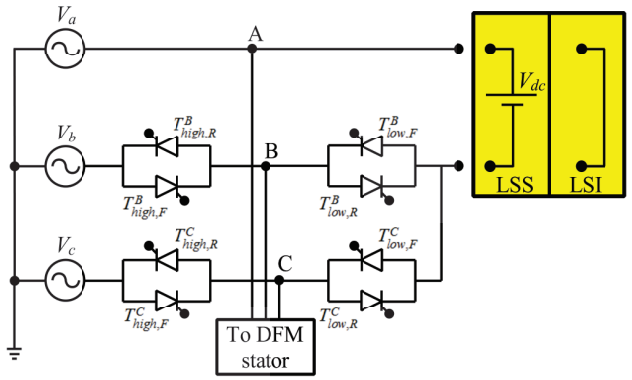

Figure 2. Eight thyristor-based transfer switch (ETB) - A-phase of the ac source is the reference for the transfer switch operation [19].

performance. Of course, for the configuration shown in this paper, a mechanical transfer switch could be used in parallel with a semiconductor transfer switch to reduce steady-state losses to a minimum [16]. Reference [17] proposed a twelve-thyristor-based (TTB) transfer switch that offers seamless transition and drive performance with an appropriate rotor-side control [18]. Alternative configurations of the thyristor-based transfer switch using eight thyristors are proposed in [19]. This paper compares the performance of the eight-thyristor-based transfer switch (ETB) with the twelve-thyristor-based transfer switch specifically under lightly-loaded conditions in the low-speed synchronous topology. Analysis shows reduction in number of thyristors for creating a transfer switch opens up the range of feasible operating conditions of the DFM over which the mode transition is accomplished seamlessly in addition to simplifying the transfer switch and decreasing the cost. An optimal non-linear controller is presented that minimizes the stator flux perturbation during the mode transition through the maximum allowable damping. Finally, an alternative transfer switch topology is proposed that is applicable for the LSS topology with even lesser number of thyristors eliminating the limitations on operating conditions for a seamless transition in the low-speed-to-high-speed mode transition. Experimental results are presented to verify the operation of the eight-thyristor-based transfer switch using an off-the-shelf 1 HP, 220V/150V, 4 pole, 1800 rpm doubly-fed machine.

II. Eight-Thyristor-Based Transfer Switch Operation and Control in the LSS Topology

Typically, fully controllable switches such as IGBTs add degrees of freedom in a power electronic converter design. On the contrary, semi-controllable switches such as thyristors (SCR) act as a constraint when used to design systems by using the turn-off functionality. Eliminating SCRs from the TTB transfer switch improves the operational flexibility of the switched-DFM drive. The eight-thyristor-based (ETB) transfer switch is shown in Fig. 2. The A-phase of the DFM is chosen as the reference for the transfer switch operation based on the advantages presented in [19]. SCRs $T^B_{high,F}$, $T^B_{high,R}$, $T^C_{high,F}$, and $T^C_{high,R}$ form the high-speed SCR bank for the transfer switch while SCRs $T^B_{low,F}$, $T^B_{low,R}$, $T^C_{low,F}$, and $T^C_{low,R}$ form the low-speed SCR bank. Turing ON the high-speed SCR bank connects the DFM stator to the ac source. The SCRs conduct for half of the ac source fundamental time period. The losses in these SCRs in steady state are predominantly the conduction losses that can be minimized using parallel mechanical switches. Alternatively, turning the low-speed SCR bank ON either connects the DFM stator to a dc source in the LSS topology or shorts the stator together in the LSI topology. In the LSS topology, for a balanced three phase stator winding of the DFM, the current in the A-phase is twice that of the currents in B and C-phases. Removing the anti-parallel SCRs from the A-phase of the TTB transfer switch reduces the conduction loss in the transfer switch in the LSS topology by two-thirds. In the LSI topology, the conduction loss in the ETB transfer switch is two-thirds in comparison to the TTB transfer switch. However, the SCRs in the ETB transfer switch must be rated to withstand the ac source line-to-line voltages instead of the ac source phase voltages as in the TTB transfer switch. In Sec. II-A an analytical framework is developed to compare the performance of the two transfer switches during a low-speed-to-high-speed mode transition in the LSS topology. Sections II-B and II-C shows the operational flexibilities of the ETB transfer switch over the TTB transfer switch under different drive torque conditions. Sec. II-D presents an optimal control policy for the rotor d-axis current that maximizes the stator flux damping during the mode transition.

A. Analytical framework for evaluation of the low-speed-to-high-speed mode transition in the LSS topology

The feasibility of a seamless low-speed-to-high-speed mode transition in the LSS topology is dependent on the drive torque demand. This section introduces an analytical framework that is used in the later sections to evaluate and compare the performances of the ETB and the TTB transfer switches. With the DFM stator initially connected to the dc source, the low-speed SCR-bank is ON. The stator current vector $\bar{i}_s$ and the stator voltage are stationary relative to the ABC stator winding axis as shown in Fig. 3. Connecting the A-phase of the stator to the positive polarity and B and C-phases to the negative polarity of the dc source enforces the stator voltage vector orientation along the A-phase axis. Under steady-state condition, the stator current vector is also directed towards the A-phase axis. The incoming ac source voltage vector $\overline{v_{ac}}$ rotates in ABC-phase sequence at the grid frequency ω_{ac} relative to the stationary reference frame. The blue sector represents the feasible region for the incoming ac source voltage vector that ensures natural commutation for all outgoing SCRs of the low-speed SCR bank in the TTB transfer switch. Reducing the number of thyristors to eight extends the feasible region to the green sector as described in [19]. Prior to the mode transition, the orientation of the stator flux vector $\bar{\psi}_s$ is dependent on the operating drive torque τ, the normalized dc source voltage v_{dc} and the designed stator flux magnitude

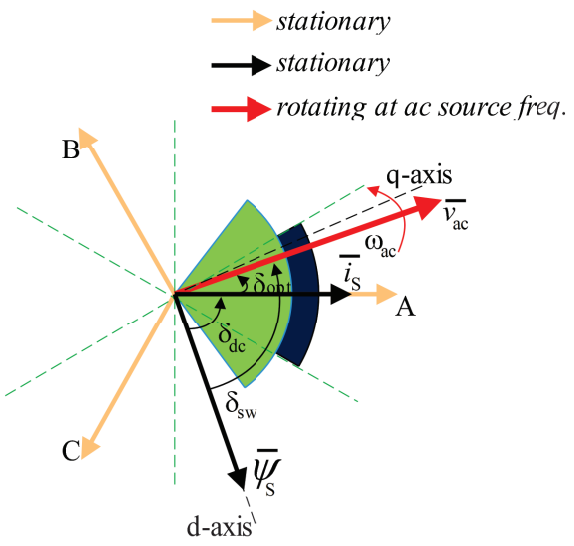

Figure 3. Commutation diagram during low-speed-to-high-speed mode transition under rated drive torque condition. Turning ON the high-speed SCR bank of the ETB transfer switch when the ac source voltage vector is within the green sector naturally turns OFF the low-speed SCR bank. The corresponding region for the TTB transfer switch is shown in blue.

in the low-speed mode ψ_s and is given by

$$\delta_{dc} = \arcsin \frac{\tau r_s}{v_{dc}\psi_s}, \tag{1}$$

where δ_{dc} represents the angle between the stator flux vector and the stator voltage vector in the low-speed mode.

Minimum perturbation in the stator flux during mode transition is achieved by connecting the ac source to the stator at the instant when the incoming ac voltage vector is at an angle δ_{sw} relative to the stator flux vector $\bar{\psi}_s$ [17], where

$$\delta_{sw} = \arccos\left(v_{dc}\cos\delta_{dc}\right). \tag{2}$$

Therefore, the desired angle for the incoming ac voltage vector relative to the A-phase axis at the instant of mode transition is given by

$$\delta_{opt} = \delta_{sw} - \delta_{dc}. \tag{3}$$

Based on the chosen transfer switch topology, the feasible region for δ_{opt} is bounded by the requirement of the natural commutation of the outgoing SCRs in the low-speed SCR bank, which is represented as

$$\delta_{opt} \in [-\epsilon, \epsilon]. \tag{4}$$

For the TTB transfer switch, $\epsilon = 30°$ [17] as represented by the blue sector while for the ETB transfer switch [19]

$$\epsilon = 60° - \arcsin\left(\frac{v_{dc}}{\sqrt{3}}\right), \tag{5}$$

as represented by the green sector where the peak phase voltage of the ac source is chosen as the base voltage for normalization. Assuming a high current controller bandwidth for the rotor currents and a high mechanical time constant, the trajectory of the stator flux after the dc-to-ac source transition is governed by [20]

$$\frac{1}{\omega_{ac}}\frac{d}{dt}\begin{bmatrix}\psi_s\\ \delta\end{bmatrix} = \begin{bmatrix} -\frac{r_s}{x_s}\psi_s + \cos\delta \\ 1 - \frac{1}{\psi_s}\sin\delta + \frac{1}{\psi_s^2}r_s\tau\end{bmatrix} + \begin{bmatrix}\frac{r_s x_m}{x_s}i_{rd}\\ 0\end{bmatrix} \tag{6}$$

where the state variables are the stator flux magnitude ψ_s and the angle between the stator flux vector and the ac source voltage δ. The parameters of the state-space representation are the normalized stator resistance r_s, stator inductance x_s, and the mutual inductance x_m of the DFM. To ensure a bumpless transition at the shaft, the drive torque τ needs to be maintained constant during the mode transition. The rotor d-axis current i_{rd} is the only available control input that affects the state trajectory during the mode transition. The steady-state operating point of the DFM in the high-speed mode can be calculated equating (6) to zero.

During the mode transition, the DFM must be operated within the allowable stator and rotor currents ratings that implies

$$i_{sd}^2 + i_{sq}^2 \le 1 \tag{7}$$

and

$$i_{rd}^2 + i_{rq}^2 \le I_{rpu}^2, \tag{8}$$

where I_{rpu} represents the normalized rated rotor current relative to the stator current rating. The rotor q-axis current component is represented by i_{rq} while i_{sd} and i_{sq} represent the d and q-axis current components for the stator. Additionally, the maximum voltage that can be impressed on the rotor is limited by the designed voltage rating of the rotor power electronic converter based on the steady-state drive design [7]. Considering v_{rd} and v_{rq} as the d and q-axis components of the rotor voltage, the limit on the allowable rotor voltage V_r enforces

$$v_{rd}^2 + v_{rq}^2 \le V_r^2. \tag{9}$$

Constraint (7) is mapped as a function f in the $\delta - \psi_s$ plane using the DFM machine model in the stator flux orientation as given in [7] by

$$f\left(\psi_s,\, \tau,\, i_{rd}\right) = \left(\frac{\psi_s - x_m i_{rd}}{x_s}\right)^2 + \left(\frac{\tau}{\psi_s}\right)^2 - 1 \le 0 \tag{10}$$

The constraint is dependent on the stator flux magnitude, drive torque, and the rotor d-axis current input. Similarly, constraint (8) is mapped as a function g in the $\delta - \psi_s$ plane by

$$g\left(\psi_s,\, \tau,\, i_{rd}\right) = i_{rd}^2 + \left(-\frac{x_s\tau}{x_m\psi_s}\right)^2 - I_{rpu}^2 \le 0. \tag{11}$$

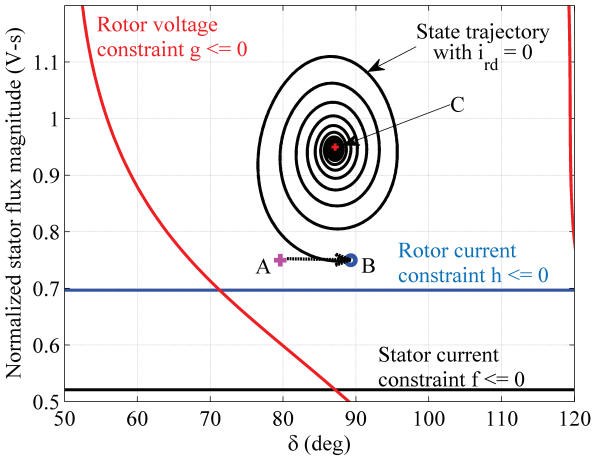

Figure 4. Stator flux trajectory during dc-to-ac source transition under rated drive torque condition lies within the constraint boundaries set by the stator current, rotor current, and the rotor power electronics voltage rating. A: Initial operating point in the $\delta - \psi_s$ plane while the DFM is operated in the low-speed mode. B: Operating point right after the mode transition. C. Steady-state operating point in the high-speed mode.

Finally, the individual components of the rotor voltage is calculated using

$$v_{rd} = r_e i_{rd} + \frac{x_m}{x_s}\cos\delta - \frac{r_s x_m}{x_s^2}\psi_s - x_e\left(\omega_s - \omega_T\right)\left(-\frac{x_s\tau}{x_m\psi_s}\right) \tag{12}$$

and

$$v_{rq} = r_r\left(-\frac{x_s\tau}{x_m\psi_s}\right) + \left(\omega_s - \omega_T\right)\left[x_e i_{rd} + \frac{x_m\psi_s}{x_s}\right] \tag{13}$$

where ω_T represents the low-speed-to-high-speed mode transition speed. The stator flux frequency is represented by ω_s and is calculated by

$$\omega_s\left(\psi_s,\ \delta,\ \tau\right) = \frac{\sin\delta}{\psi_s} - \frac{r_s\tau}{\psi_s^2}. \tag{14}$$

r_e and x_e represents the equivalent resistance and inductance and is given by

$$r_e = r_r + r_s\frac{x_m^2}{x_s^2};\ x_e = x_r - \frac{x_m^2}{x_s}. \tag{15}$$

Using (12) and (13), the rotor voltage constraint (9) is mapped as a function h in the $\delta - \psi_s$ plane and is represented by

$$h\left(\psi_s,\ \delta,\ \tau,\ i_{rd}\right) = v_{rd}^2 + v_{rq}^2 - V_r^2 \leq 0. \tag{16}$$

In the following sections, the developed model along with the constraints projected on the $\delta - \psi_s$ plane are used to compare the performance of the ETB and the TTB transfer switch during the mode transition under different operating drive torque conditions.

B. Low-speed-to-high-speed mode transition at rated drive torque condition

At the rated drive torque condition during the desired mode transition, τ equals 0.498 p.u for the example DFM as derived in [7]. The parameters of the example DFM are also given in [7]. With a dc source voltage of 0.068 p.u and a designed stator flux magnitude of 0.75 p.u, full drive torque demand sets the operating point of the DFM in the low-speed mode at $(80°,\ 0.75)$ denoted by A in the $\delta - \psi_s$ plane as shown in Fig. 4. The optimum transition instant δ_{opt} for minimizing the stator flux perturbation is calculated as $10°$ using (3). The optimum transition instant lies well within the constraint ϵ of the TTB transfer switch to enable a natural commutation of the outgoing SCRs in the low-speed SCR bank. For the ETB transfer switch, ϵ is calculated as $\sim 55°$ using (5) implying that the dc to ac source transition is equally feasible at the optimum transition instant. After the source transition, the operating point is placed instantly at $(90°,\ 0.75)$ denoted by B in the $\delta - \psi_s$ plane. The stator flux transition dynamics follows (6) to reach the steady state in the ac source connected mode denoted by C. The stator flux transition trajectory shown in Fig. 4 is with the d-axis rotor current input set to zero.

The constraints from the stator current rating, rotor current rating, and the voltage rating of the rotor power electronic drive, using (10), (11), and (16) respectively, are mapped to the $\delta - \psi_s$ plane. The entire state trajectory remains within the constraint boundaries during the mode transition ensuring that the low-speed-to-high-speed mode transition is achievable seamlessly for the example DFM under rated drive torque condition using either of the ETB or the TTB transfer switches. Additionally, the rotor d-axis current can be commanded to damp the oscillations in the stator flux magnitude using a full-state feedback controller [18] or an optimally damped control law as will be discussed in Sec. II-D.

C. Low-speed-to-high-speed mode transition in the LSS topology at low drive torque condition

Under lightly loaded condition, the demanded drive torque is lower than the rated value for the DFM. For example, assuming a drive torque demand τ to be 0.174 p.u (35% of the rated torque in the low-speed mode) for the example DFM, the operating point of the DFM in the low-speed mode is at $(20°,\ 0.75)$ denoted by D in the $\delta - \psi_s$ plane as shown in Fig. 5. The optimum transition instant δ_{opt} for minimizing the stator flux perturbation is calculated as $66°$ using (3). The optimum transition instant is not feasible to be achieved using either of the TTB or the ETB transfer switches as this would violate the condition required to satisfy the natural commutation for the outgoing SCRs. The condition is depicted in the vector diagram shown in Fig. 6 where the optimum transition instant from the perspective of minimizing stator flux transients is achieved when the ac source voltage vector is at $\overline{v_{ac}}$ while lying outside the feasible sectors for natural commutation of the outgoing SCRs. To ensure natural commutation of the SCRs, the transition must be initiated at $\overline{v_{ac}'}$ for the ETB transfer switch and at $\overline{v_{ac}''}$ for the TTB transfer switch.

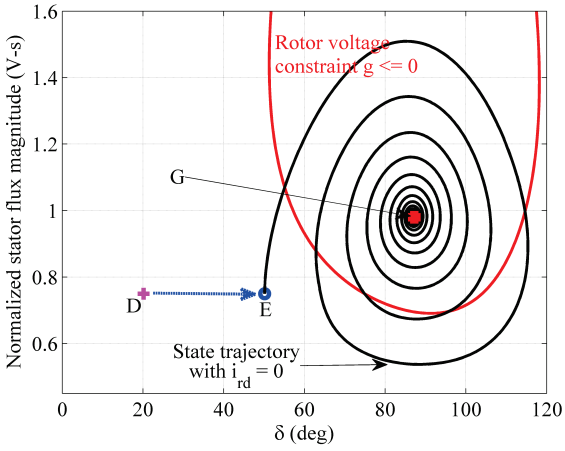

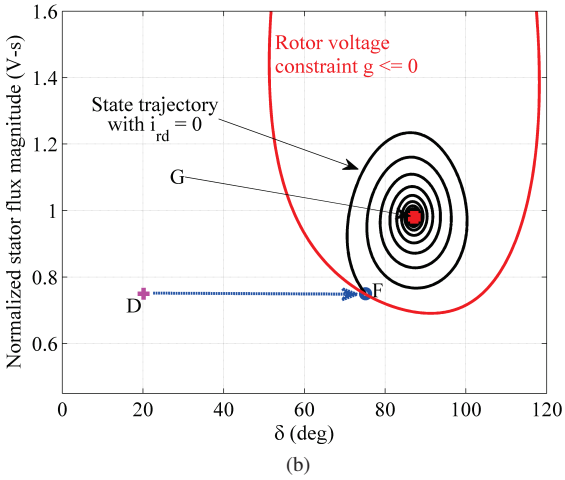

Figure 5. Stator flux trajectory during dc-to-ac source transition under low drive torque condition (35% of the rated drive torque). D: Initial operating point in the $\delta - \psi_s$ plane while the DFM is operated in the low-speed mode. G: Steady-state operating point in the high-speed mode. (a) TTB transfer switch: E is the operating point right after the mode transition. $DE = 30°$ (b) ETB transfer switch: F is the operating point right after the mode transition. $DF = 55°$

The natural commutation of the SCR constraint enforces the operating point of the DFM after the source transition to be at $(50°, 0.75)$ denoted by E for the TTB transfer switch and at $(75°, 0.75)$ denoted by F for the ETB transfer switch as shown in Fig. 5(a) and (b) respectively.

Using (6), the stator flux trajectory with zero d-axis rotor current input for these two initial conditions are also shown in Fig. 5. The stator flux magnitude swing is 20% higher for the TTB transfer switch in comparison to the ETB transfer switch. A higher flux swing results in saturation of the magnetic circuit of the DFM affecting the overall performance of the DFM. Moreover, the TTB transfer switch will not be able to provide a seamless torque at the shaft during the mode transition. This can be observed by superimposing the rotor converter voltage constraint of $V_r = 0.52$ p.u in the $\delta - \psi_s$ plane of

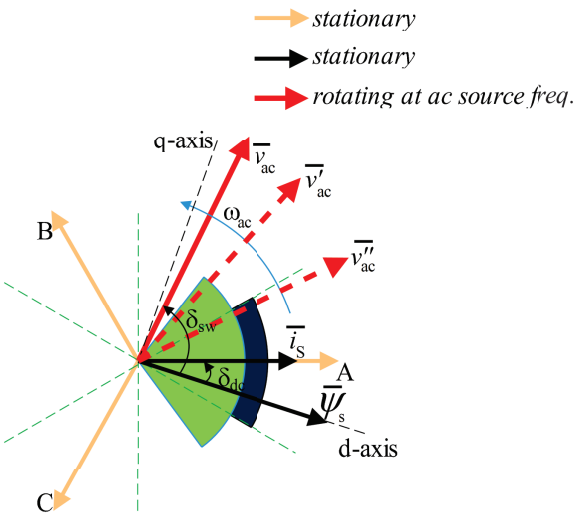

Figure 6. Commutation diagram during low-speed-to-high-speed mode transition under low drive torque condition. From the DFM perspective, a dc-to-ac source transition instant when the ac source voltage vector is at $\overline{v_{ac}}$ incurs least perturbation in the stator flux. However, constraints for the natural commutation of the outgoing SCRs in the low-speed SCR bank enforces the transition instant to be at $\overline{v'_{ac}}$ for the ETB transfer switch and at $\overline{v''_{ac}}$ for the TTB transfer switch respectively.

Fig. 5(a). Multiple points in the state trajectory including the initial condition of E lies outside the rotor voltage constraint boundary implying that the rotor voltage will be limited during the mode transition. The limited rotor voltage leads to limited q-axis rotor current and consequently a bump in the drive torque. The constraints for the stator current rating and the rotor current rating are much relaxed in the $\delta - \psi_s$ plane and do not directly affect the drive performance under low drive torque condition. For the ETB transfer switch, all the points in the state trajectory including the initial condition of F lies within the rotor voltage constraint boundary implying that a seamless transition can be achieved with zero d-axis rotor current command.

D. Optimum rotor d-axis current input to minimize stator flux transients

The analysis shown in Sec. II-B and Sec. II-C explicitly sets the rotor d-axis current to zero to emphasize on the state trajectories during the mode transition with zero control input. However, appropriate rotor d-axis current damps the oscillations in the stator flux within the allowable bounds of the stator current, rotor current and the rotor converter voltage rating. Multiple approaches can be used to optimize the d-axis rotor current input based on the system-specific requirement. For example, one approach is to maximize the damping of the stator flux during a low-speed-to-high-speed mode transition.

Two steps are involved to compute the optimum rotor d-axis current that maximizes the stator flux damping. First, identification of the correct polarity of i_{rd} that can maintain stability of the DFM during the mode transition and second,

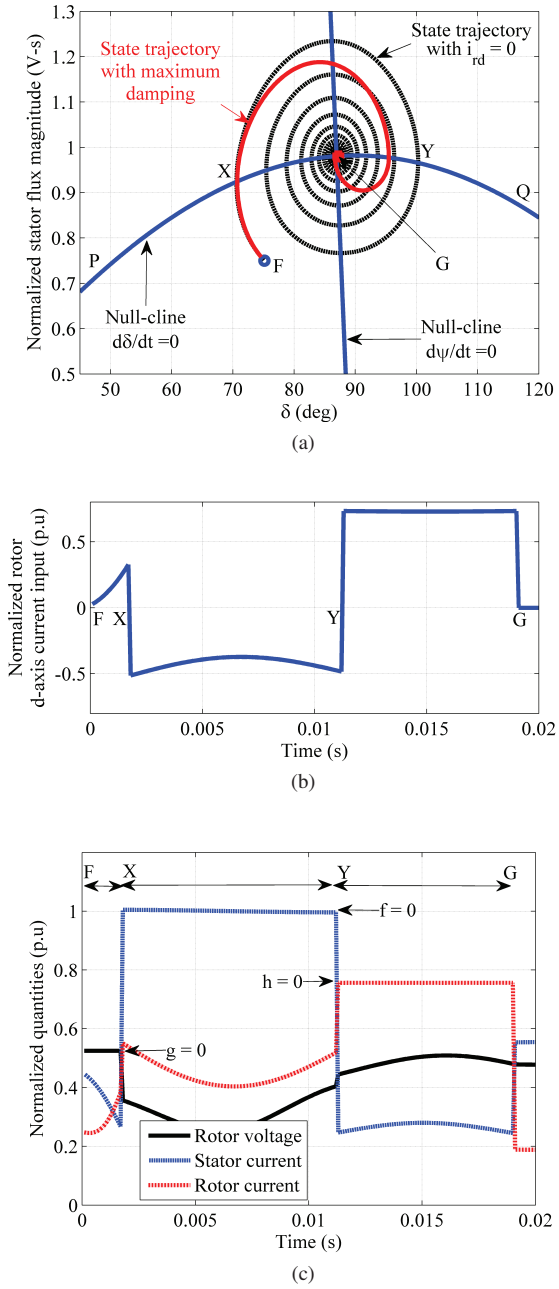

Figure 7. Maximizing rotor d-axis current input to damp stator flux oscillation during dc-to-ac source transition. (a) Comparison of the stator flux trajectories with and without d-axis rotor current damping under light drive torque condition. (b) Optimal rotor d-axis current input ensuring that the constraints of the stator current, rotor current, and rotor converter voltage rating are satisfied at all operating points of the damped trajectory. (c) The constraint functions f, g, and h during the dc-to-ac source transition that remain within the respective limits for the example DFM.

maximizing i_{rd} that can be impressed along the state trajectory to damp the stator flux within the allowable limits. As the rotor d-axis current affects the state trajectory only along the ψ_s axis, as evident from (6), the stabilizing polarity of i_{rd} at each instant is such that the state trajectory is driven inwards towards the steady-state operating point G in Fig. 5. The null-cline obtained by equating $d\delta/dt$ in (6) to zero is shown as by the line segment PQ in Fig. 7(a). For the operating points below the null-cline PQ, a non-negative rotor d-axis current results in forcing the state flux to inner trajectories in the phase plane. Conversely for the operating points above the null-cline PQ, a non-positive rotor d-axis current ensures that the stator flux is drawn towards the inner trajectories in the phase plane.

The maximum rotor d-axis current that can be impressed to damp the stator flux transients is governed by the constraints described by (10), (11), and (16). For the example DFM with a 35% drive torque demand during the mode transition, the optimum d-axis rotor current is shown in Fig. 7(b). During the sections FX and YG in the state trajectory, a positive d-axis rotor current is commanded while in the section XY, a negative rotor d-axis current is used to damp the stator flux oscillation. The magnitude of the rotor d-axis current is governed by the rotor voltage constraint in the section FX as shown in Fig.7(c). In the section XY, the magnitude of the rotor d-axis current is set by the stator current constraint while in the section YG, the limit on the rotor current plays the dominant role in determining the magnitude of the rotor d-axis current. The above outlined procedure can be repeated to find the optimal d-axis rotor current that provides maximum stator flux damping for other drive torque conditions.

III. Alternative Thyristor-Based Transfer Switch for LSS Topology: Operation and Control

The minimum drive torque requirement for a torque-bumpless transition from low-speed mode to high-speed mode can be eliminated for the LSS topology using an alternative transfer switch topology as shown in Fig. 8. In this transfer switch configuration, two of the stator windings (for example, A and B-phases) conduct equal and opposite currents as set by dc source while the current in the C-phase is zero in the low-speed mode. In steady-state condition, the stator current vector $\bar{i}'_s$ in the low speed mode is given by

$$\bar{i}'_s = \left(\frac{3}{2} - j\frac{\sqrt{3}}{2}\right)\frac{v'_{dc}}{2r_s} = \frac{\sqrt{3}}{2}\frac{v'_{dc}}{r_s}\angle -30^\circ \qquad (17)$$

where v'_{dc} is the dc source voltage. On the contrary, the stator current vector in the low-speed mode for the TTB or the ETB transfer switch is given by

$$\bar{i}_s = \frac{v_{dc}}{r_s}. \qquad (18)$$

This requires that the dc source voltage v'_{dc} is marginally increased such that the magnitude of the stator current vector remains identical for all the transfer switch topologies achieving identical stator flux magnitude. Therefore,

$$v'_{dc} = \frac{2}{\sqrt{3}}v_{dc} \qquad (19)$$

The operation of the DFM in the low-speed mode remains same as the TTB or the ETB transfer switch except that the

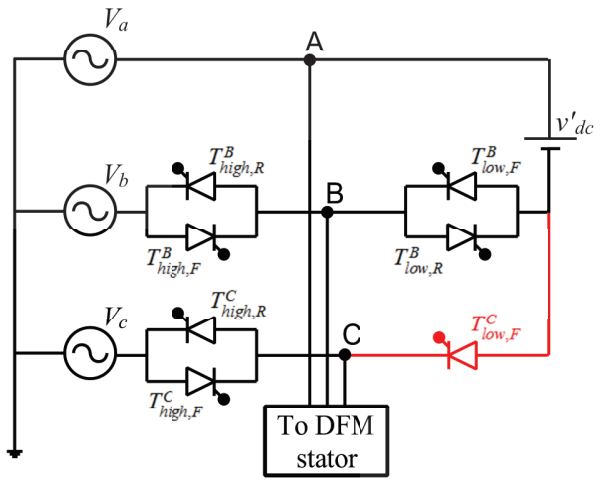

Figure 8. An alternative transfer switch topology for a switched-DFM drive in the LSS topology that achieves seamless dc-to-ac-source transition over a wider range of drive torque demand compared to the ETB transfer switch with $\epsilon \approx 90°$. SCR $T^C_{low,F}$ does not conduct in the low-speed mode but aids in current commutation during ac-to-dc source transition.

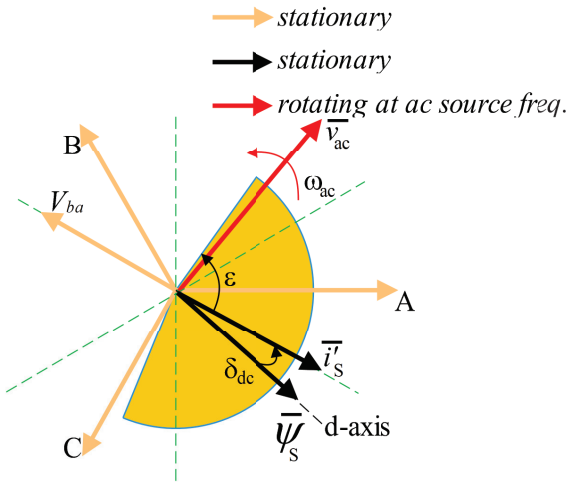

Figure 9. Commutation diagram during low-speed-to-high-speed mode transition under low drive torque condition for the alternative proposed transfer switch. A wide range of allowable ac source voltage vector location is feasible during a dc-to-ac source transition shown by the yellow sector to meet the natural commutation requirement of the SCR $T^B_{low,R}$. The dc source voltage vector and the steady state stator current vector is at an angle $-30°$ relative to the stator A-phase winding axis.

stator current vector $\bar{i}'_s$ is oriented along $-30°$ relative to the stator A-phase winding axis as shown in Fig. 9. With the current in the B-phase stator winding being negative, for a successful commutation of the $T^B_{low,R}$ thyristor during low-speed-to-high-speed mode transition, the required constraint on the ac source voltage is given by

$$v_{ba} < -v'_{dc}. \tag{20}$$

The possible commutation region for the incoming ac source voltage vector is shown by the yellow sector in Fig. 9 with the ϵ being calculated as

$$\epsilon = 90° - \arcsin\left(\frac{v'_{dc}}{\sqrt{3}}\right). \tag{21}$$

Equation (21) is similar to (5) but with a wider range of allowable stator voltage vector location during low-speed-to-high-speed mode transition. For the example DFM, ϵ is calculated as $87°$ implying that the dc-to-ac source transition can be initiated for any positive drive torque.

In the absence of the SCR $T^C_{low,F}$ in Fig. 8, the ac-to-dc source transition can only be performed when the stator current in the C-phase is zero. Presence of the SCR $T^C_{low,F}$ assists during the ac-to-dc source transition without affecting the dc-to-ac source transition.

IV. Experimental Result

The experimental setup used to verify the operation of the proposed transfer switch has been described in [19]. The 146 V (line-to-line, rms), 40 Hz ac grid created using two parallel-operated synchronous generators provides the overall power to the switched-DFM drive. The stator of the DFM is connected to a prototype ETB transfer switch that can toggle the stator connection to the ac source during high-speed mode operation. The drive is configured in the LSS topology where a separate 20 V dc source supplies the stator during low-speed mode. In the transfer switch, diodes are placed in series with each SCR to enable faster turn off during mode transition. An RC snubber of 330 Ω and 6.8 nF is connected in parallel with the SCRs to limit the dv/dt stress. The rotor of the DFM is connected to the ac grid using a back-to-back converter configuration using two Texas Instruments High Voltage Motor Control & PFC Developer's Kits. The DFM is connected to a load generator (PMSG), which can operate with different load torque profiles. The mode transition is initiated by a hysteresis comparator that compares the rotor speed to high and low threshold set points.

Figure 10 shows the stator flux transition in the $\delta - \psi_s$ plane during dc-to-ac source change over in the LSS topology. A_1, A_2, and A_3 represent three initial operating points in the low-speed mode under three different drive torque demands, which are 56%, 74%, and 94% of the low-speed drive torque capability respectively. The ETB transfer switch enforces the operating points to move to B_1, B_2, and B_3 after the stator of the DFM is connected to the ac grid such that the outgoing low-speed SCR bank undergoes natural commutations. Finally, the stator flux settles down to steady-state operating points C_1, C_2, and C_3 respectively. As expected from the analytical framework, experimental results show similar behavior in the stator flux transition during low-speed-to-high-speed mode transition. Under lower drive torque demand, A_1 in this case, the transition instance is set by the SCR commutation requirement rather than optimum instance for least perturbation of the

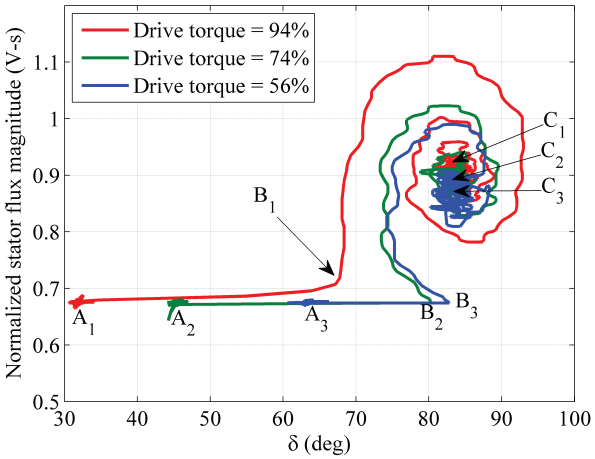

Figure 10. Experimental result: Stator flux transition during low-speed-to-high-speed mode transition under different drive torque condition. A_1, A_2, and A_3: Initial operating point with the DFM stator connected to the dc source. B_1, B_2, and B_3: Operating point post transition to the ac source. C_1, C_2, and C_3: Steady-state operating point in the high speed mode.

stator flux after transition.

V. Conclusions

This paper presented performance comparison of three different topologies of solid-state transfer switches for a switched-DFM drive under low drive torque condition in the LSS topology. The seamless transition of the DFM along with the natural commutation of the SCR-based transfer switch must be simultaneously satisfied for a smooth or "bumpless" mechanical operation of the switched-DFM drive over a wide range of drive torque-speed requirements. Reducing the number of SCRs in the transfer switch result in removing turn-off constraints that enables seamless mode transition over a wide range of drive torque demands. Optimal d-axis rotor current command damps stator flux transition within the allowable limits as set by the stator current, rotor current, and the rotor converter voltage rating. As the associated power converter for a switched-DFM drive required to handle only one-third of the shaft mechanical power over the complete speed range, the overall drive scheme becomes attractive for many high power applications including propulsion. Many variations on the transfer switch are possible, including parallel mechanical switches or relays to reduce steady state power consumption. The analytical framework in this paper can be extended to other arrangements to provide convenient transfer switch properties for any application.

Acknowledgment

This research was performed with support from the Skoltech-MIT SDP Program, and The Grainger Foundation.

References

[1] S. Kouro, J. Rodriguez, B. Wu, S. Bernet, and M. Perez, "Powering the future of industry: High-power adjustable speed drive topologies," *Industry Applications Magazine, IEEE*, vol. 18, no. 4, pp. 26–39, July 2012.

[2] J. Sayago, T. Bruckner, and S. Bernet, "How to select the system voltage of mv drives - a comparison of semiconductor expenses," *Industrial Electronics, IEEE Transactions on*, vol. 55, no. 9, pp. 3381–3390, Sept 2008.

[3] J. Rodriguez, S. Bernet, B. Wu, J. Pontt, and S. Kouro, "Multilevel voltage-source-converter topologies for industrial medium-voltage drives," *Industrial Electronics, IEEE Transactions on*, vol. 54, no. 6, pp. 2930–2945, Dec 2007.

[4] J. Rodriguez, B. Wu, S. Bernet, N. Zargari, J. Rebolledo, J. Pontt, and P. Steimer, "Design and evaluation criteria for high power drives," in *Industry Applications Society Annual Meeting, 2008. IAS '08. IEEE*, Oct 2008, pp. 1–9.

[5] S. Bernet, "Recent developments of high power converters for industry and traction applications," *Power Electronics, IEEE Transactions on*, vol. 15, no. 6, pp. 1102–1117, Nov 2000.

[6] Z. Chen, J. Guerrero, and F. Blaabjerg, "A review of the state of the art of power electronics for wind turbines," *Power Electronics, IEEE Transactions on*, vol. 24, no. 8, pp. 1859–1875, Aug 2009.

[7] A. Banerjee, M. Tomovich, S. B. Leeb, and J. L. Kirtley, "Power converter sizing for a switched doubly fed machine propulsion drive," *Industry Applications, IEEE Transactions on*, vol. 51, no. 1, pp. 248–258, Jan 2015.

[8] A. Banerjee, S. B. Leeb, and J. L. Kirtley, "Switched doubly-fed machine for ship propulsion," *Electric Machines Technology Symposium, ASNE*, May 2014.

[9] B. Wu, *High-Power Converters and AC Drives*. IEEE Press, March 2006.

[10] A. Banerjee, S. B. Leeb, and J. L. Kirtley, "Seamless grid interaction for a switched doubly-fed machine propulsion drive," in *Electric Machines Drives Conference (IEMDC), 2015 IEEE International*, May 2015.

[11] L. Morel, H. Godfroid, A. Mirzaian, and J.-M. Kauffmann, "Double-fed induction machine: converter optimisation and field oriented control without position sensor," *Electric Power Applications, IEE Proceedings -*, vol. 145, no. 4, pp. 360–368, Jul 1998.

[12] S. B. Leeb, J. L. Kirtley, W. Wichakool, Z. Remscrim, C. N. Tidd, J. A. Goshorn, K. Thomas, R. W. Cox, and R. Chaney, "How much dc power is necessary?" *Naval Engineers Journal*, vol. 122, no. 2, pp. 79–92, 2010.

[13] A. Banerjee, S. B. Leeb, and J. L. Kirtley, "A comparison of switched doubly-fed machine drive topologies for high power applications," in *Electric Machines Drives Conference (IEMDC), 2015 IEEE International*, May 2015.

[14] F. Bonnet, L. Lowinsky, M. Pietrzak-David, and P.-E. Vidal, "Doubly fed induction machine speed drive for hydro-electric power station," in *Power Electronics and Applications, 2007 European Conference on*, Sept 2007, pp. 1–9.

[15] X. Yuan, J. Chai, and Y. Li, "A converter-based starting method and speed control of doubly fed induction machine with centrifugal loads," *Industry Applications, IEEE Transactions on*, vol. 47, no. 3, pp. 1409–1418, May 2011.

[16] B. Tian, C. Mao, J. Lu, D. Wang, Y. He, Y. Duan, and J. Qiu, "400 v/1000 kva hybrid automatic transfer switch," *Industrial Electronics, IEEE Transactions on*, vol. 60, no. 12, pp. 5422–5435, Dec 2013.

[17] A. Banerjee, A. Chang, K. Surakitbovorn, S. B. Leeb, and J. L. Kirtley, "Bumpless automatic transfer for a switched-doubly-fed-machine propulsion drive," *Industry Applications, IEEE Transactions on*, vol. 51, no. 4, pp. 3147–3158, July 2015.

[18] A. Banerjee, M. Tomovich, S. B. Leeb, and J. L. Kirtley, "Control architecture for a switched doubly fed machine propulsion drive," *Industry Applications, IEEE Transactions on*, vol. 51, no. 2, pp. 1538–1550, March 2015.

[19] A. Banerjee, S. B. Leeb, and J. L. Kirtley, "Solid state transfer switch topologies for a switched doubly-fed machine drive," *Power Electronics, IEEE Transactions on*, vol. PP, no. 99, pp. 1–1, 2015.

[20] ——, "Transient performance comparison of switched doubly-fed machine propulsion drives," in *Transportation Electrification Conference and Expo (ITEC), 2015 IEEE*, June 2015.